JOURNAL OF CATALYSIS 141, 700–712 (1993)

Preparation and Characterisation of Montmorillonite-Supported Palladium Hydrogenation Catalysts Possessing Molecular Sieving Properties

M. CROCKER, R. H. M. HEROLD, J. G. BUGLASS, AND P. COMPANJE

Koninklijke/Shell-Laboratorium, Amsterdam (Shell Research B.V.), Postbox 3003, 1003 AA Amsterdam, The Netherlands

Received September 2, 1992; revised January 4, 1993

Highly dispersed palladium metal has been deposited in the interlayer space of montmorillonite clay by the reduction of intercalated palladium complexes. The use of the highly electrophilic Pd(II) precursor complexes $[Pd(PPh_3)(NCMe)_3]^{2+}$ and $[PdL_4]^{2+}$ (L = NCMe, $(CH_3)_2CO$) is shown to facilitate the reduction step under very mild conditions (0°C; MeOH as reaction medium). TEM analysis of reduced $[Pd(PPh_3)(NCMe)_3]^{2+}$/clay and $[Pd(NCMe)_4]^{2+}$/clay samples reveals that the palladium is present largely in the interlamellar regions of the clay, in the latter case as particles of platelet morphology. A procedure for depositing palladium metal exclusively in the interlamellar region of the clay particles is also described. Transmission electron micrographs of the resulting material (containing 1 wt% Pd) reveal a very narrow size distribution for the palladium crystallites formed, the median particle diameter being ca. 8 Å. Consistent with this is an observed basal spacing of 8–10 Å for the intercalated regions of the clay. Molecular sieving effects are observed when this material is used as a catalyst for the hydrogenation of cyclic and monosubstituted alkenes of varying critical dimension. In contrast, catalysts prepared by simple reduction of Pd(II) complexes homogeneously dispersed in montmorillonite show significantly less shape selectivity towards olefinic reactants.

INTRODUCTION

Smectite clays are increasingly attracting interest as supports for metal and metal complex catalysts. These minerals, which are layered lattice silicates, can be readily functionalised, either via ion-exchange with a positively charged metal complex or with organic ligands to which a metal can subsequently be attached (*1–5*). Equally important, clays possess a number of physical and chemical properties which potentially permit modification of the selectivity and activity of supported metals and metal complex catalysts. These characteristics include:

(i) the laminar structure of the clay, theoretically enabling selective adsorption of molecules based on size or shape (i.e., a molecular sieving effect); additionally, there exists the potential that transition state selectivity may arise in reactions occurring in the sterically restricted interlamellar regions;

(ii) the negative charge of the silicate sheets, potentially resulting in the polarisation of adsorbed molecules;

(iii) the high Brønsted acidity of some dehydrated clays with the consequent potential for acid promotion of reactions requiring both metal complex and acid functionalities, and for the stabilisation of cationic hydride intermediates (relative to their homogeneous analogues) in catalytic systems where proton dissociation can occur.

Several of these features have been demonstrated during studies directed at the hydrogenation of unsaturated molecules catalysed by interlamellar metal complex catalysts (*1–13*). To date there have been fewer reports concerning the preparation and catalytic properties of metal particles dispersed on swelling clay supports, al-

0021-9517/93 $5.00

though the use of pillared clays containing noble metals and synthetic mica–montmorillonite clays for hydrocracking and hydroisomerisation applications has been reported (*14*). Additionally, Giannelis *et al.* (*15*) have observed an unusual selectivity towards branched products in the Fischer–Tropsch hydrocarbon synthesis when an alumina-pillared montmorillonite containing encapsulated crystalline ruthenium aggregates was used as catalyst. Shimazu *et al.* (*16*) have reported the synthesis of reduced ruthenium–hectorite catalysts with various interlamellar distances, and in a study of the activity of these materials in the hydrogenation of olefins have observed molecular sieving effects. There have also been recent reports concerning the preparation of dispersed platinum (*17*), copper (*18, 19*), and nickel (*19*) metal particles supported on montmorillonite.

In the present paper we describe the preparation, under very mild conditions, of highly dispersed palladium in the interlamellar region of montmorillonite clay via hydrogen reduction of intercalated electrophilic Pd(II) complexes. Initial studies directed towards the hydrogenation of olefins indicate that these materials possess molecular sieving properties.

METHODS

Starting Materials

Sodium montmorillonite (MM–Na^+) was obtained via purification of bentonite (BDH) according to the method of van Olphen (*20*). The approximate anhydrous unit cell formula determined on the basis of elemental analysis and ^{27}Al NMR MAS spectroscopy was $Na_{0.62}[Al_{3.16}Fe^{III}_{0.36}Fe^{II}_{0.08}Mg_{0.40}](Si_{7.86}Al_{0.14})O_{20}(OH)_4$; the measured cation exchange capacity (CEC) of the clay was 82 meq/100 g. $[Pd(NCMe)_4][BF_4]_2$ and $[Pd(PPh_3)(NCMe)_3][BF_4]_2$ were prepared as described in the literature (*21*). Olefins were of the highest purity available and were degassed before use. Acetonitrile was dried over CaH_2, acetone over K_2CO_3, and methanol (MeOH) over NaOMe. Solvents were distilled under nitrogen immediately prior to use. Unless otherwise stated, all manipulations were performed under an atmosphere of dry nitrogen using standard Schlenk techniques or a Braun model MB 200 glovebox.

Intercalation of Pd(II) Derivatives in Montmorillonite

$[Pd(PPh_3)(NCMe)_3]^{2+}$ and $[Pd(NCMe)_4]^{2+}$. Vacuum-dried MM–Na^+ was first suspended in acetonitrile (ca. 20 ml MeCN/g clay) with stirring overnight. The requisite amount of $[Pd(PPh_3)(NCMe)_3][BF_4]_2$ or $[Pd(NCMe)_4][BF_4]_2$ was then added to the swollen clay and stirring was continued for 3–4 h. The clay product was isolated by filtration, washed thoroughly with acetonitrile and then ether, and dried under vacuum.

$[Pd\{(CH_3)_2CO\}_4]^{2+}$. A solution of $[Pd\{(CH_3)_2CO\}_4][BF_4]_2$ (prepared *in situ* by stirring $Pd(OAc)_2$ (0.202 g; 0.9 mmol) and $HBF_4 \cdot Et_2O$ (1.8 mmol) in acetone (25 ml)) was added to a slurry of vacuum-dried MM–Na^+ (2.0 g; 1.64 meq) in acetone (30 ml). The mixture was stirred for 4 h. The yellow-brown product was isolated by filtration, washed thoroughly with acetone and dried under vacuum.

Reduced materials were prepared by stirring a cooled (0°C) methanol suspension of the intercalated clay for 30 min under an atmosphere of hydrogen (1 atm).

Preparation of Catalyst **1**

MM–Na^+ (5.00 g; 4.1 meq) was ion-exchanged with $[Pd(PPh_3)(NCMe)_3][BF_4]_2$ (0.332 g; 0.50 mmol) as described above. The clay was then stirred for 15 min in CH_2Cl_2 (50 ml) in which $P(o\text{-}CH_3C_6H_4)_3$ (0.061 g; 0.20 mmol) had been dissolved. The clay product was isolated by filtration, washed with CH_2Cl_2, and dried under vacuum. Reduction of this material, as described above, afforded catalyst **1**.

Characterisation of Clay Samples

Elemental analysis of samples for Pd was carried out using X-ray fluorescence (XRF) spectroscopy to within an accuracy of ±10% (relative). For infrared analysis, self-supporting wafers were prepared and mounted in an evacuable stainless steel cell. Spectra were recorded using a Digilab FTS 15 (Biorad) FT-IR spectrometer. XPS spectra were recorded on a Kratos XSAM 800 spectrometer employing the C 1*s* line (284.6 eV) as a binding energy standard. Elemental concentrations obtained from the XPS spectra are estimated to be accurate to within ± 20% (relative). X-ray diffraction measurements were performed with a Philips PW 1820 powder diffractometer using Cu$K\alpha$ radiation.

Samples for transmission electron microscopy were ground with a mortar and pestle, suspended in *n*-butanol, and then sprayed onto a continuous, ultrathin carbon film supported on a Cu grid. The samples were analysed in a Philips 400T transmission electron microscope operating at 100 kV. The maximum image resolution of 0.4 nm could only be achieved in the thinnest regions of the sample. In general, clay samples suffer damage when bombarded by the intense electron beam in the microscope. In this work, however, the samples showed surprising beam stability.

The local elemental composition of the clay was determined using light element energy dispersive X-ray microanalysis and was performed using a Link Analytical detector. Average palladium particle diameters for each loading were calculated using the formula $d_{avg} = (\Sigma n \cdot d_i^3)/(\Sigma n \cdot d_i^2)$, where d_i is the diameter of particle i measured from the micrograph and n is the number of crystallites in the range d and $d + 10$ Å (*22*).

Hydrogenation of Olefins

All hydrogenation experiments were conducted using a constant pressure apparatus operating at 1 atm. In a typical procedure, the catalyst sample (equivalent to 0.01 mmol palladium) was stirred in methanol (30 ml) cooled to 0°C for 1 h under nitrogen. The resulting suspension was injected into the hydrogenation apparatus and was stirred for a further 30 min under hydrogen (also at 0°C). The hydrogenation reaction was initiated by injecting the olefin (2.0 mmol) into the reaction vessel, the volume of hydrogen consumed being measured as a function of time. Additionally, 100-μl portions of the solution were withdrawn at regular intervals for GLC analysis (HP-1 cross-linked dimethylsilicone column; heptane as internal standard). At termination of the experiment the catalyst was recovered by filtration (porosity 4 frit) and the solution analysed by GLC. The rate of olefin consumption was generally found to be linear for at least the first 60% of the reaction.

RESULTS AND DISCUSSION

Intercalation of Pd(II) Complexes in Montmorillonite

For the purposes of this study, three palladium complexes were employed: $[Pd\{(CH_3)_2CO\}_4][BF_4]_2$, $[Pd(NCMe)_4][BF_4]_2$, and $[Pd(PPh_3)(NCMe)_3][BF_4]_2$ (*21*), intercalation of the cations into montmorillonite being achieved via ion exchange in the appropriate solvent (see Experimental Section). The use of rather electrophilic Pd(II) complexes facilitates the deposition of palladium metal under mild reducing conditions (*vide infra*). Indeed, the intercalated homoleptic complexes $[Pd\{(CH_3)_2CO\}_4][BF_4]_2$ and $[Pd(NCMe)_4][BF_4]_2$ showed considerable moisture sensitivity (particularly the latter), decomposing slowly in air to afford palladium metal.

Analytical data obtained on the ion-exchanged clays are summarised in Table 1. Comparisons of the surface palladium concentrations, determined by XPS, with those determined for the bulk (using XRF) show reasonable agreement, after allowing for the experimental error associated with the

TABLE I

Elemental Analysis, XPS, XRD, and Diffuse Reflectance Data for Palladium Complexes Intercalated in Montmorillonite

Complex	[Pd] (wt%)		$3d_{5/2}$ B. E. (eV)	FWHM (eV)	Basal spacing (Å)	λ_{max} (nm)
	XRF	XPS				
$[Pd\{(CH_3)_2CO\}_4]^{2+}$						
(i) Before redn.	3.9	3.0	337.1	3.8	13.0	396
(ii) After redn.	—	2.2	335.4	3.0	12.3	—
$[Pd(NCMe)_4]^{2+}$						
(i) Before redn.	1.0	—	—	—	—	—
(ii) After redn.	—	0.8	335.7	4.1	11.3	—
$[Pd(PPh_3)(NCMe)_3]^{2+}$						
(i) Before redn.	2.2	3.0	337.5	3.6	15.8	—
(ii) After redn.	—	2.9	336.0	3.5	16.0	—
$[Pd(PPh_3)(NCMe)_3]^{2+}$ [a]						
(i) Before redn.	1.1	1.2	337.3	3.3	11.8	—
(ii) After redn.	—	1.1	336.0 337.3	3.3	10.1	—

[a] Catalyst **1** (MM–Na^+ intercalated with $[Pd(PPh_3)(NCMe)_3]^{2+}$, subsequently treated with $P(o\text{-}C_6H_4CH_3)_3$ in CH_2Cl_2).

two techniques (see Experimental Section). This finding is consistent with a homogeneous dispersion of the metal complexes throughout the clay, although in itself cannot be regarded as absolute proof.

Powder X-ray diffraction data obtained on the materials (after evacuation) show increases in the basal spacing of the clay from 9.6 Å (for vacuum-dried MM–Na^+) to 13.0 Å for the product obtained with $[Pd\{(CH_3)_2CO\}_4]^{2+}$, and 15.8 Å for that obtained with $[Pd(PPh_3)(NCMe)_3]^{2+}$. These figures are indicative of intercalation of the palladium complexes in the montmorillonite clay, such that the metal–ligand bonds are parallel to the silicate sheets with the vacant d_{z^2} orbital perpendicular to the *ab*-plane. Indeed, previous studies have shown that this orientation is preferred for square planar Pd(II) (*23*), Pt(II) (*17*), and Cu(II) (*24*) complexes adsorbed on montmorillonite.

It should be noted that exposure of vacuum-dried MM–Na^+ to acetone, followed by evacuation, produces a material having a basal spacing of 12.6 Å, corresponding to the formation of a one-layer complex between the acetone and the Na^+ ions of the clay (*25*). In this instance the interlayer (clearance) spacing of the clay is essentially determined by the dimensions of the $-CH_3$ group; indeed a basal spacing of 12.6 Å is also observed for montmorillonite intercalated (at high loadings) with $[Pd(NCMe)_4]^{2+}$ (*26*). The slightly larger basal spacing of 13.0 Å observed for MM–Na^+ intercalated with $[Pd\{(CH_3)_2CO\}_4]^{2+}$ suggests that the interlayer spacing of the clay is determined here by the effective thickness of the complex (rather than by the residual acetone solvent); in order to accommodate four acetone ligands around the metal centre in a square planar geometry, a slight out-of-plane distortion of the ligands is needed, thereby increasing the necessary clearance spacing relative to a simple $-CH_3$ group.

In the case of MM–Na^+ intercalated with $[Pd(PPh_3)(NCMe)_3]^{2+}$, the observed basal spacing of 15.8 Å clearly indicates that the spacing of the clay layers is determined by

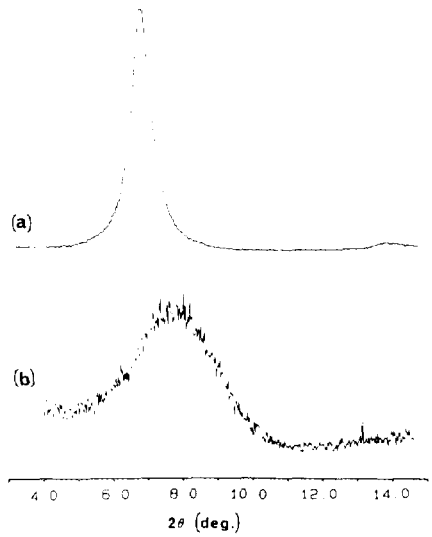

FIG. 1. X-ray diffractograms of MM—Na^+/[Pd $\{(CH_3)_2CO\}_4]^{2+}$ before (a) and after (b) reduction.

the size of the triphenylphosphine ligand. The somewhat broader appearance of the d_{001} reflection of this material, in comparison with the [Pd$\{(CH_3)_2CO\}_4]^{2+}$ intercalate (Fig. 1 and 2), is probably a result of the lower metal complex loading of the former, resulting in less effective pillaring of the clay and hence a greater variation in interlayer spacings.

Infrared spectral data for the ion-exchanged clays proved uninformative, the presence of residual solvent in the clay masking bands due to the intercalated complexes. Thus even after evacuation at 80°C, the spectrum of [Pd$\{(CH_3)_2CO\}_4]^{2+}$.intercalated in MM–Na^+ showed strong bands at 1712 and 1692 cm^{-1}, which are attributed to adsorbed acetone interacting with Na^+ ions (*25*). However, the diffuse reflectance spectrum of the adsorbed acetone complex showed a well defined maximum at 396 nm, consistent with the presence of a PdO_4 (O = oxygen donor ligand) species (*27, 28*).

Reduction of Intercalated Pd(II) Complexes

All three intercalated complexes undergo immediate reduction when exposed to hydrogen at 0°C in the presence of methanol. Furthermore, the complexes are unstable in the presence of methanol alone, their high electrophilicity resulting in dehydrogenation of the solvent:

$$Pd^{2+} + CH_3OH \rightarrow Pd^0 + 2\,H^+ + CH_2 = O. \quad (1)$$

This finding may be rationalised in terms of a mechanism in which methoxide ion attack on the starting complex generates a Pd^+–OCH_3 species; hydrogen transfer to the metal (for which there is ample precedent (*29*)) with concomitant liberation of CH_2O (detected by GC) would then generate a Pd^+–H species which upon proton loss would afford zero-valent palladium.

In contrast, the complex [Pd(PPh_3) $(NCMe)_3][BF_4]_2$ was found to be stable in nonprotic solvents such as CH_2Cl_2 in the presence of hydrogen, while thermogravimetry and differential thermal analysis revealed that [Pd$(PPh_3)(NCMe)_3]^{2+}$ adsorbed on MM–Na^+ does not undergo reduction in the presence of hydrogen below 280°C.

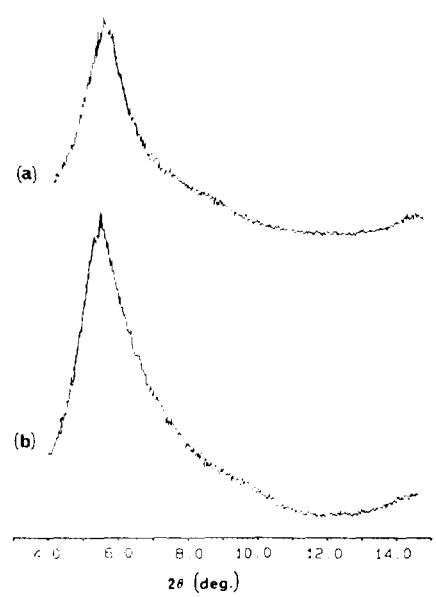

FIG. 2. X-ray diffractograms of MM–Na^+/ [Pd$(PPh_3)(NCMe)_3]^{2+}$ (2.2 wt% Pd) before (a) and after (b) reduction.

However, even freshly prepared methanol solutions of $[Pd(PPh_3)(NCMe)_3][BF_4]_2$ were found to contain colloidal palladium, light scattering indicating an average particle size of 30–40 nm. The less electrophilic bis (phosphine) and tris(phosphine) complexes $[Pd(PPh_3)_x(NCMe)_{4-x}][BF_4]_2$ (x = 2, 3) (*21*) were, in contrast, found to be stable in methanol solution and did not undergo reduction at room temperature in the presence of hydrogen. Furthermore, these complexes were found to be inactive for the hydrogenation of alkenes and alkynes at room temperature.

XPS spectra of the intercalated clays prior to reduction show binding energies for the Pd $3d_{5/2}$ level in the range 337.1–337.5 eV, characteristic of palladium in the divalent state. As expected, reduction is accompanied by a lowering of the binding energies, the $3d_{5/2}$ level reaching 335.4–335.7 eV for the reduced homoleptic samples (Table 1). Significantly, binding energies for reduced MM–Na^+/$[Pd(PPh_3)(NCMe)_3]^{2+}$ samples are, at 336.0 eV, somewhat higher than for the former materials. Assuming a binding energy for metallic palladium of 335.6 eV (*30*), the slightly higher binding energies observed here are probably attributable to the small size of the palladium particles at high dispersion, and imply a higher degree of dispersion for the reduced MM–Na^+/$[Pd(PPh_3)(NCMe)_3]^{2+}$ materials than for their homoleptic analogues. Several studies (*31*, *32*) on silica-supported palladium have previously shown that palladium binding energies shift to higher values with decreasing particle size (for particles of $\leq$2.0–3.0 nm). Verification of these findings is provided by the results of TEM analyses performed on these materials (*vide infra*).

A difference is also observed between the X-ray diffractograms of reduced MM–Na^+/$[Pd\{(CH_3)_2CO\}_4]^{2+}$ (3.9 wt% Pd) and MM–Na^+/$[Pd(PPh_3)(NCMe)_3]^{2+}$ (2.2 wt% Pd). The d_{001} reflection of the former material is significantly broader (with a corresponding decrease in intensity) than for its unreduced precursor (Fig. 1), indicating that reduction results in a loss in the long range structural regularity of the clay. Additionally, XPS data indicate that reduction results in an apparent decrease in the surface palladium concentration (from 3.0 to 2.2 wt%). Although this finding has not been studied further, it may be a consequence of palladium leaching during the reduction step, possibly in the form of $[Pd\{(CH_3)_2CO\}_4]^{2+}$ molecules which were strongly physisorbed on the clay (as the BF_4^- salt), as opposed to being ion-exchanged.

In contrast, reduction of intercalated $[Pd(PPh_3)(NCMe)_3]^{2+}$ does not result in significant broadening of the d_{001} reflection of the clay (Fig. 2), consistent with the presence of intercalated palladium particles possessing a narrow particle size distribution (*vide infra*). Materials prepared using lower palladium loadings (e.g., $[Pd(PPh_3)(NCMe)_3]^{2+}$ at a loading of 1 wt% Pd) gave diffractograms indicative of a less ordered structure, both before and after reduction.

In order to gain further insight into the form and location of the palladium particles present, a TEM analysis was performed on reduced MM–Na^+/$[Pd(NCMe)_4]^{2+}$ and MM–Na^+/$[Pd(PPh_3)(NCMe)_3]^{2+}$ samples having Pd loadings of 1.0 and 2.2 wt%, respectively. The results of these studies have been reported elsewhere (*26*) and only those observations relevant to the current work are summarised here. For the reduced MM–Na^+/$[Pd(NCMe)_4]^{2+}$ clay, noteworthy is the finding that the palladium in this material is present as particles of platelet morphology sandwiched between the clay layers, particle widths being typically a factor of three smaller than the diameters measured along the longest axis. The observation of a nonspherical form for the palladium particles suggests that particle morphology is strongly influenced by the presence of the layered clay structure. Indeed, it can be speculated that the particles may be kinetically inhibited from developing a more spherical morphology (thermo-

dynamically more stable due to the minimisation of surface free energy) by the constraints imposed by the silicate sheets. Additionally, the possibility that the palladium particles may be stabilised with respect to a more spherical morphology as a consequence of interactions with the clay surface (a thermodynamic effect) cannot be discounted.

For the reduced MM–Na^+/$[Pd(PPh_3)(NCMe)_3]^{2+}$ material no definitive conclusions can be drawn regarding the morphology of the palladium crystallites present owing to their small size, although the few larger particles observed appeared to be nonspherical. However, for both samples it can be concluded that the particles are located principally between the clay layers. Significant aggregation of the palladium particles at the sheet edges was not observed for either sample, while for the reduced MM–Na^+/$[Pd(NCMe)_4]^{2+}$ clay only the platelet morphology was observed.

For the MM–Na^+/$[Pd(PPh_3)(NCMe)_3]^{2+}$ sample (2.2 wt% Pd) a rather narrow particle size distribution is observed (Fig. 3a), the median and average particle diameters being 20–30 Å and ca. 40 Å, respectively. The median particle diameter is significantly larger than the interlamellar spacing of 6.4 Å deduced from the X-ray diffractogram of the clay, a result which could be explained if the particles were indeed to possess a platelet morphology. Additionally, it should be noted that the basal spacing observed by X-ray diffraction actually corresponds to a value averaged over the intercalated and nonintercalated regions of the clay (*33*), i.e., the interlamellar spacing corresponding to the intercalated regions of the clay could in actuality be slightly larger than 6.4 Å.

For the reduced MM–Na^+/$[Pd(NCMe)_4]^{2+}$ (1 wt.% Pd) material the palladium is less highly dispersed (see Fig. 3b), reflected in the median and average particle diameters of 90–120 Å and ca. 140 Å, respectively. Since both materials were

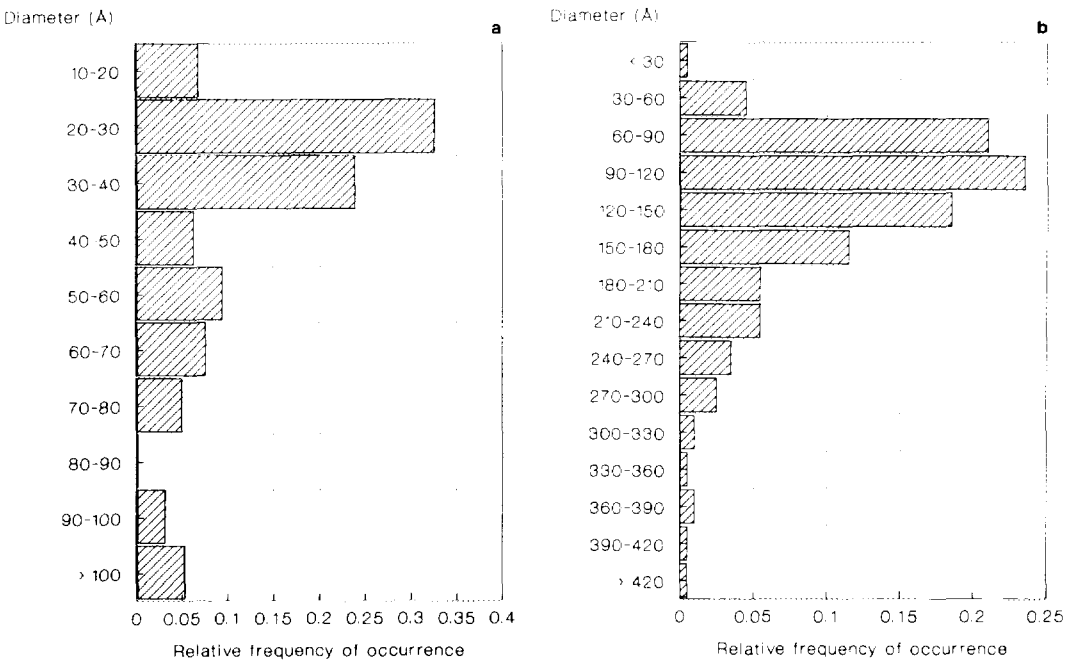

FIG. 3. Particle size distributions of palladium crystallites in (a) reduced MM–Na^+/$[Pd(PPh_3)(NCMe)_3]^{2+}$ (2.2 wt% Pd) and (b) reduced MM–Na^+/$[Pd(NCMe)_4]^{2+}$ (1.0 wt% Pd).

reduced under identical conditions, these findings graphically illustrate the important role that the nature of the precursor Pd(II) complex (and its associated reduction behaviour) can play in determining the degree of dispersion of the supported metal.

Preparation and Characterisation of a Shape-Selective Hydrogenation Catalyst

Several previous studies have demonstrated the shape-selective properties of hydrogenation catalysts based on clays intercalated with metal complexes (*2–4, 6, 10, 13*) and metal particles (*16*). However, a number of problems exist in such systems which can be expected to limit their shape selectivity. First, swelling clays have a tendency to be turbostratic, i.e., the clay sheets are randomly stacked with respect to the in-plane *a*- and *b*-axes of neighboring sheets. In consequence, catalyst molecules located towards the edges of the clay sheets occupy exposed positions and would be expected to be undiscriminating with respect to the size of approaching reactants. The same can also be said of catalytic sites located on the exposed surface of the outermost clay layers. For the montmorillonite used in this work a surface area of 31 m^2/g was measured, while a total layer area of 725 m^2/g was calculated on the basis of the unit cell formula derived from chemical analysis (*34*). It follows, therefore, that approximately 5% of the total area (and hence 5% of the exchange sites) is associated with the external surface of the clay. Furthermore, these external sites are more accessible to reactants (substrates) than are their interlamellar counterparts. Catalytic functionalities introduced onto these sites will therefore contribute more significantly to the overall substrate conversion than would be expected on the basis of their concentration alone.

An additional problem is the fact that clays intercalated with metal complex catalysts are sometimes interstratified, with the result that interlayer spacings can be rather larger or smaller than the average value indicated by the observed d_{001} X-ray reflection (*33*). Pinnavaia (*1*) has pointed out that as a consequence of this, efficient catalytic discrimination among substrates on the basis of size or shape can be expected only when the differences in the critical dimensions are larger than the spread in interlayer spacings.

In an attempt to overcome these limitations and prepare a hydrogenation catalyst possessing molecular sieving properties, the following strategy was adopted. MM–Na^+ was ion-exchanged with $[Pd(PPh_3)(NCMe)_3][BF_4]_2$ in acetonitrile to a palladium loading of 0.1 mmol/g, and the clay, after drying, briefly treated with excess tri-o-tolylphosphine in CH_2Cl_2. Under these conditions the bulky phosphine (cone angle = 194° (*35*)) is unable to penetrate between the layers of the partially swollen clay and reacts only with $[Pd(PPh_3)(NCMe)_3]^{2+}$ located in the accessible exterior regions of the clay particles, forming the bis(phosphine) complex $[Pd(PPh_3)\{P(o\text{-}CH_3C_6H_4)_3\}(NCMe)_2]^{2+}$ (*21*). Treatment of the product clay with hydrogen in methanol at 0°C results in the formation of dispersed palladium metal in the interlamellar regions of the clay (via reduction of the mono(phosphine) complex), while the less electrophilic bis(phosphine) complex remains intact. XPS data confirm the presence of both Pd(O) and Pd(II) in the product, **1** (Fig. 4), the single $3d_{5/2}$ peak observed at 337.3 eV for the nonreduced material becoming, after reduction, a doublet corresponding to binding energies of 337.3 and 336.0 eV (Fig. 5).

A transmission electron micrograph of **1** (Fig. 6) shows features similar to those previously discussed for the reduced MM–$Na^+/[Pd(PPh_3)(NCMe)_3]^{2+}$ (Pd = 2.2 wt%) material, the main difference being the rather smaller average particle diameter observed for the material with the lower metal loading (i.e., **1**). Micrographs of **1** reveal a very narrow size distribution for the palladium crystallites formed (Fig. 7), with 73%

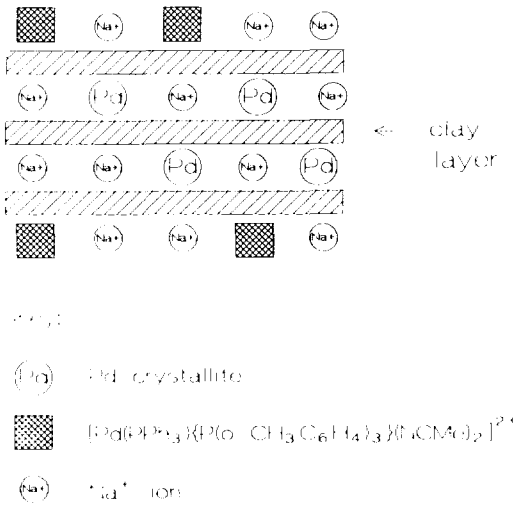

FIG. 4. Schematic representation of the structure of catalyst **1**. Note that (solvated) protons, formed according to Eq. (1), may also be present, bound to the interlayer cation sites.

of the crystallites having a diameter of less than 20 Å. (It should be noted that this percentage represents a minimum value due to the difficulty in detecting such small particles.) A median particle size of ca. 8 Å was found, with the average particle size being 14 Å. The presence of crystallites between the clay layers is also indicated, an interlayer spacing of 8–10 Å being observed by TEM for the intercalated regions of the clay.

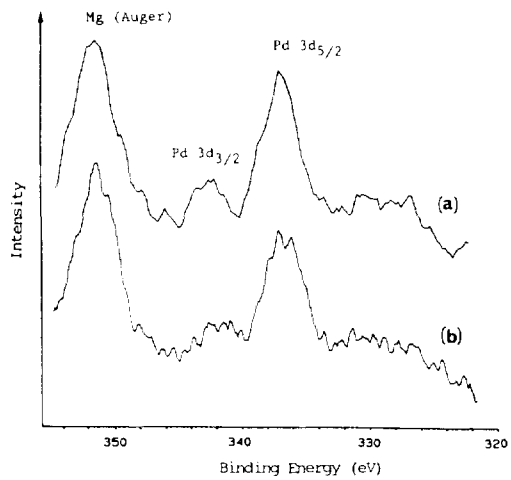

FIG. 5. XPS spectrum of **1** before (a) and after (b) reduction.

Olefin Hydrogenation Studies

Olefin hydrogenation studies were carried out using catalyst **1** in methanol. At this relatively low palladium loading (corresponding to substitution of ca. 25% of the Na^+ ions in MM–Na^+), the clay largely retains its swelling properties. This is confirmed by X-ray powder diffraction, which reveals a basal spacing of 16.6 Å for **1** swollen in methanol, compared to a basal spacing of 17.1 Å for MM–Na^+ in methanol. Since the thickness of a silicate sheet is 9.6 Å, the swelling of **1** corresponds to an average interlamellar spacing of 7.0 Å.

In order to assess the potential of **1** for the shape-selective hydrogenation of olefins, hydrogenation rates were measured for a number of olefins ranging in their critical dimensions. Control experiments were also performed using reduced $[Pd(NCMe)_4]^{2+}$ on MM–Na^+ (1.0 wt% Pd) (**2**), as well as a commercial sample of 1 wt% Pd on alumina (**3**). Results are summarised in Table 2. The most striking result is obtained for cycloheptene: while hydrogenation proceeds readily over catalysts **2** and **3**, no activity is observed with **1** (although it is active for cyclopentene and cyclohexene hydrogenation), this despite the fact that the critical dimensions for the three cycloalkenes are somewhat similar (5.0 Å for cyclohexene versus 5.4 Å for cycloheptene on the basis of van der Waals' radii).

This finding suggests that in addition to the interlamellar distance, the lateral distance between the solvated Na^+ ions residing on the ion-exchange sites in the clay is also, in this instance, an important parameter with respect to the accessibility of the interlamellar region. On the basis of the total layer area calculated for the clay and the measured cation exchange capacity (CEC), it can be calculated (*34*) that the average distance between Na^+ ions in the MM–Na^+

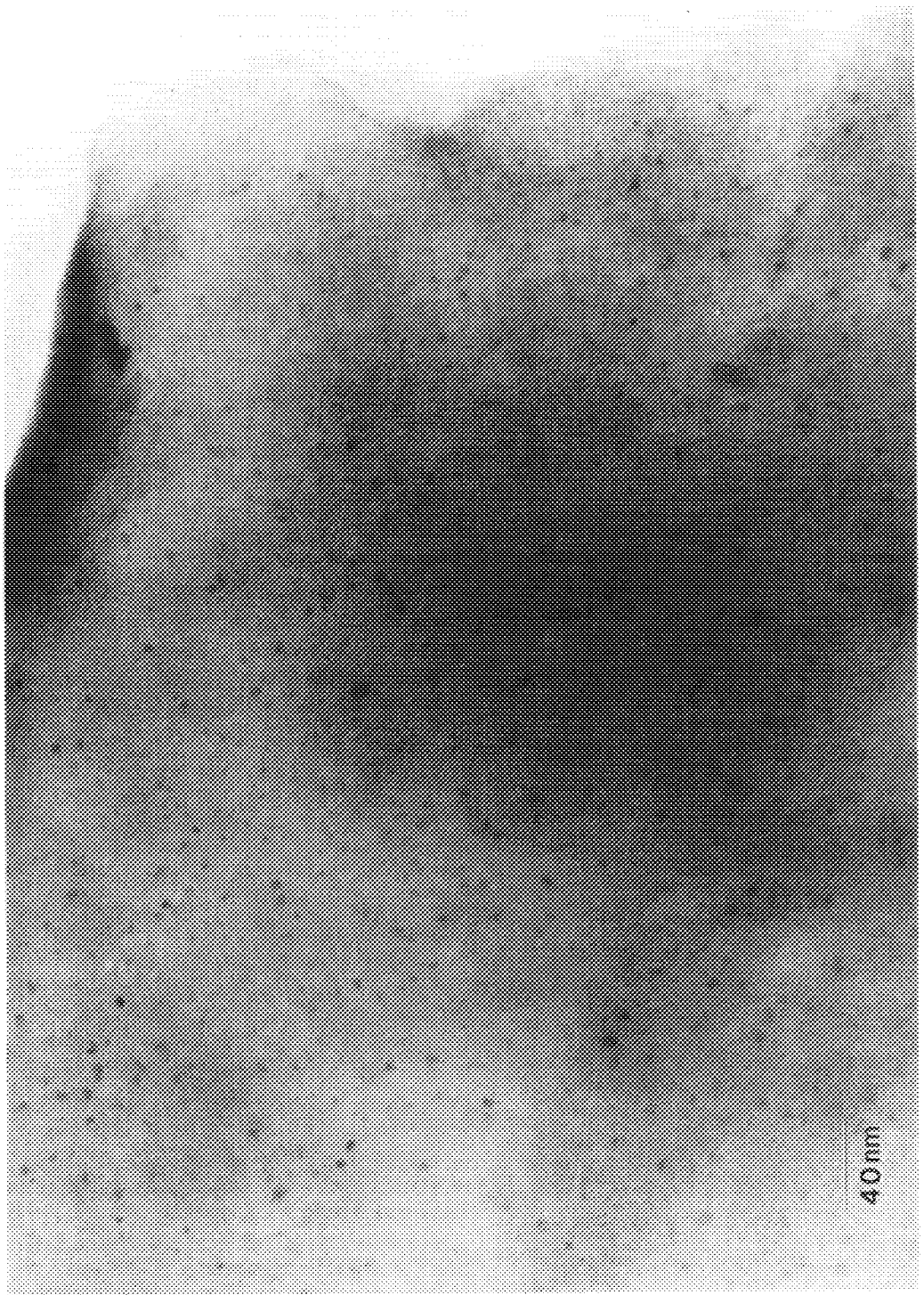

FIG. 6. Transmission electron micrograph of **1**.

TABLE 2

Olefin Hydrogenation Using Heterogeneous Palladium Catalysts[a]

Olefin	Critical dimension (Å)[b]	Catalyst					
		1		2[d]		3[e]	
		Rate[c]	Rel. rate	Rate[c]	Rel. rate	Rate[c]	Rel. rate
Cyclopentene	4.9	89	6	—	—	364	5
Cyclohexene	5.0	15	1	—	—	156	2
Cycloheptene	5.4	0	0	79	1	77	1
Styrene	3.0	368	25	1800	23	2050	27
3,3-Dimethyl-1-butene	6.0	40	3	995	13	3600	47

[a] Olefin = 2.0 mmol, Pd = 0.01 mmol, solvent = MeOH (30 ml), T = 273 K.

[b] Calculated using the Sybil molecular modelling package (Triphos Associates Inc.); the error is estimated to be ± 0.1 Å.

[c] mol alkane/(mol Pd · h).

[d] Prepared by reduction of MM–Na^+ ion-exchanged with $[Pd(NCMe)_4]^{2+}$ (1.0 wt% Pd).

[e] 1 wt% Pd on alumina.

used in this work is 12.1 Å. Taking the diameter of a methanol molecule to be ca. 4 Å, it can be seen that the effective lateral opening between adjacent solvated Na^+ ions reduces to around 4–5 Å (assuming octahedral coordination of the ions). Clearly then, significant barriers to diffusion must exist in the *ab*-plane, in addition to those in planes perpendicular to the clay layers (determined by the interlayer spacing).

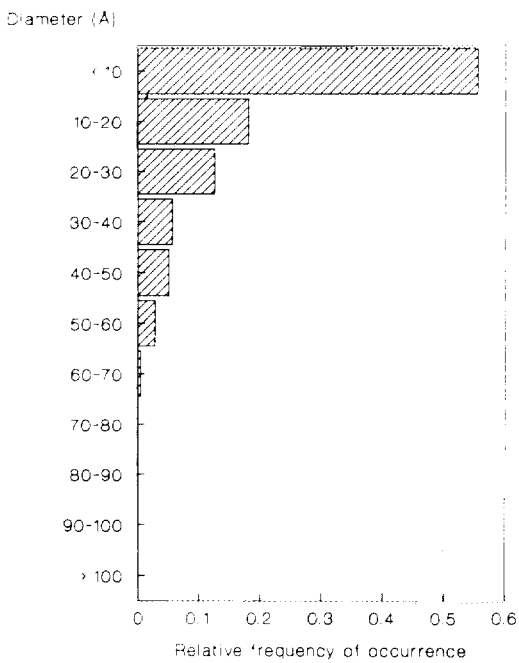

FIG. 7. Particle size distribution of palladium crystallites in **1**.

It is also instructive to compare the relative rates of styrene and 3,3-dimethyl-1-butene hydrogenation observed for the catalysts. While 3,3-dimethyl-1-butene is hydrogenated at about twice the rate for styrene using Pd/Al_2O_3, in the presence of the reduced MM–Na^+/$[Pd(NCMe)_4]^{2+}$ catalyst the ordering is reversed, suggesting the involvement of (weak) shape selective effects. For catalyst **1** the result is more clear-cut: styrene is hydrogenated almost ten times as fast as 3,3-dimethyl-1-butene. In this case a correlation is observed with the critical dimensions of the two olefins; while that for 3,3-dimethyl-1-butene is calculated to be 6.0 Å, the critical dimension of styrene is essentially determined by the thickness of the benzene ring (3.0 Å).

Comparison of the styrene hydrogenation rates observed for the three catalysts reveals that **2** and **3** show similar activity, being somewhat more active than catalyst

1. This finding can be attributed to additional diffusional restrictions in the phosphine-treated clay catalyst, resulting from the presence of the bulky (nonreduced) Pd(II) mixed phosphine complex molecules residing on ion-exchange sites at the clay platelet edges. Additionally, as intimated above, the potentially most active hydrogenation sites in **1**, i.e., those on the exterior surface of the clay particles, are in this case absent.

CONCLUSIONS

In this study it has been shown that highly dispersed palladium metal can be deposited onto montmorillonite clay via methanol reduction of intercalated palladium complexes. The use of highly electrophilic Pd(II) complexes facilitates the reduction step under very mild conditions. The ease with which many late transition metal alkoxide complexes undergo hydrogen transfer reactions suggests that this methodology could find more general application in the preparation of supported metal catalysts.

Palladium particles intercalated in montmorillonite have been imaged using transmission electron microscopy and found to possess a rather unusual platelet morphology. The generality of this finding is at present uncertain, since we are unaware of any studies in which metal particles intercalated in other types of layered structure (e.g., graphite, layered phosphates) have been directly observed. Additionally, it was found from a TEM analysis of reduced samples of $[Pd(PPh_3)(NCMe)_3]^{2+}$ exchanged into montmorillonite at loadings of 1.1 and 2.2 wt% Pd that the mean particle diameter of the palladium crystallites increases with the loading.

Deposition of palladium metal in the interlamellar region of montmorillonite clay in a highly selective manner is shown to be feasible, providing that the exterior (i.e., extralamellar) Pd(II) sites are sufficiently stabilised prior to reduction of the interlamellar Pd(II). Alternatively, one could envisage a scheme in which the extralamellar palladium sites are poisoned after the reduction step. However, to date we have been unable to find a suitable poisoning agent which is both highly efficient and incapable of penetrating between the silicate sheets of the (partially pillared) clay.

Of particular interest is the observation that although the interlayer spacing in catalyst **1** is 7.0 Å in methanol, strong molecular sieving effects are observed in the hydrogenation of alkenes possessing critical dimensions smaller than this figure. Clearly, the interlayer spacing of the swollen clay is not the sole parameter which governs the accessibility of the interlayer region to the substrate; rather, we suggest that the effective pore opening is determined by a combination of the interlayer spacing and the free space between the solvated cations residing on ion exchange sites. Molecular modelling studies currently in progress may help to clarify this point.

ACKNOWLEDGMENTS

The authors thank M. Krijger and G. M. Mulder for X-ray diffraction and XPS measurements, and Dr. H. P. C. E. Kuipers for helpful discussions.

REFERENCES

1. Pinnavaia, T. J., *Science* **220,** 365 (1983).
2. Choudary, B. M., and Rao, K. K., *Tetrahedron Lett.* **33,** 121 (1992).
3. Choudary, B. M., Ravi Kumar, K., and Lakshmi Kantam, L., *J. Catal.* **130,** 41 (1991).
4. Choudary, B. M., Mukkanti, K., and Subba Rao, Y. V., *J. Mol. Catal.* **48,** 151 (1988).
5. Shimazu, S., Ishida, T., and Uematsu, T., *J. Mol. Catal.* **55,** 353 (1989).
6. Shimazu, S., Teramoto, W., Iba, T., Miura, M., and Uematsu, T., *Catal. Today* **6,** 141 (1989).
7. Raythatha, R., and Pinnavaia, T. J., *J. Catal.* **80,** 47 (1983).
8. Pinnavaia, T. J., *ACS Symp. Ser.* **192,** 241 (1982).
9. Raythatha, R., and Pinnavaia, T. J., *J. Organomet. Chem.* **218,** 115 (1981).
10. Pinnavaia, T. J., Raythatha, R., Guo-Shuh Lee, J., Halloran, L. J., and Hoffman, J. F., *J. Am. Chem. Soc.* **101,** 6891 (1979).
11. Quayle, W. H., and Pinnavaia, T. J., *Inorg. Chem.* **18,** 2840 (1979).
12. Pinnavaia, T. J., and Welty, P. K., *J. Am. Chem. Soc.* **97,** 3819 (1975).

13. Miyazaki, T., Tsuboi, A., Urata, H., Suzuki, H., Morikawa, Y., Moro-oka, Y., and Ikawa, T., *Chem. Lett.*, 793 (1985).
14. See, for example: (a) Matsuda, T., Fuse, T., and Kikuchi, E., *J. Catal.* **160,** 38 (1987); (b) Giannetti, J. P., and Fisher, D. C., *ACS Symp. Ser.* **20,** 52 (1975).
15. Giannelis, E. P., Rightor, E. G., and Pinnavaia, T. J., *J. Am. Chem. Soc.* **110,** 3380 (1988).
16. Shimazu, S., Hirano, T., and Uematsu, T., *Appl. Catal.* **34,** 255 (1987).
17. Harrison, J. B., Berkheiser, V. E., and Erdos, G. W., *J. Catal.* **112,** 126 (1988).
18. (a) Ravindranathan, P., Malla, P. B., Komarneni, S., and Roy, R., *Catal. Lett.* **6,** 401 (1990); (b) Malla, P. B., Ravindranathan, P., Komarneni, S., Breval, E. and Roy, R., *J. Mater. Chem.* **2,** 565 (1992).
19. Patel, M., *X-Ray Spectrom.* **11,** 64 (1982).
20. van Olphen, H., "An Introduction to Clay Colloid Chemistry," p. 249. Wiley–Interscience, New York, 1977.
21. Sen, A., and Lai, T. W., *J. Am. Chem. Soc.* **103,** 4627 (1981).
22. Primet, M., Bassert, S. M., Garbowski, E., and Mathieu, M. V., *J. Am. Chem. Soc.* **97,** 3655 (1975).
23. Crocker, M., and Herold, R. H. M., *J. Mol. Catal.* **70,** 209 (1991).
24. Clementz, D. M., Pinnavaia, T. J., and Mortland, M. M., *J. Phys. Chem.* **77,** 196 (1973).
25. Parfitt, R. L., and Mortland, M. M., *Soil Sci. Soc. Am. Proc.* **32,** 355 (1968).
26. Crocker, M., Buglass, J. G., and Herold, R. H. M., *Chem. Mater.* **5,** 105 (1993).
27. Rasmussen, L., and Jørgensen, C., *Acta Chim. Scand.* **22,** 2313 (1968).
28. Stephenson, T. A., Morehouse, S. M., Powell, A. R., Heffer, J. P., and Wilkinson, G., *J. Chem. Soc.*, **1965,** 3632.
29. Collman, J. P., Hegedus, L. S., Norton, J. R., and Finke, R. G., "Principles and Applications of Organotransition Metal Chemistry," p. 90. University Science Books, Mill Valley, CA, 1987.
30. Pitchon, V., Guenin, M., and Praliaud, H., *Appl. Catal.* **63,** 333 (1990).
31. Takasu, Y., Unwin, R., Tesche, B., Bradshaw, A. M., and Grunze, M., *Surf. Sci.* **77,** 219 (1978).
32. Mason, M. G., *Phys. Rev. B.* **27,** 748 (1983).
33. Hendricks, S. B., and Teller, E., *J. Chem. Phys.* **10,** 147 (1942).
34. van Olphen, H., "An Introduction to Clay Colloid Chemistry," p. 254. Wiley–Interscience, New York, 1977.
35. Tolman, C. A., *Chem. Rev.* **77,** 313 (1977).